

AUTONOMOUS EXTRACTION OF GLEASON PATTERNS FOR GRADING PROSTATE CANCER USING MULTI-GIGAPIXEL WHOLE SLIDE IMAGES

Taimur Hassan¹ Ayman El-Baz² Naoufel Werghi¹

¹Khalifa University, UAE, ²University of Louisville, USA

ABSTRACT

Prostate cancer (PCa) is the second deadliest form of cancer in males. The severity of PCa can be clinically graded through the Gleason scores obtained by examining the structural representation of Gleason cellular patterns. This paper presents an asymmetric encoder-decoder model that integrates a novel hierarchical decomposition block to exploit the feature representations pooled across various scales and then fuses them together to generate the Gleason cellular patterns using the whole slide images. Furthermore, the proposed network is penalized through a novel three-tiered hybrid loss function which ensures that the proposed model accurately recognizes the cluttered regions of the cancerous tissues despite having similar contextual and textural characteristics. We have rigorously tested the proposed network on 10,516 whole slide scans (containing around 71.7M patches), where the proposed model achieved 3.59% improvement over state-of-the-art scene parsing, encoder-decoder, and fully convolutional networks in terms of intersection-over-union.

Index Terms—Prostate Cancer, Gleason Patterns, Dice Loss, Focal Tversky Loss

1. INTRODUCTION

Prostate cancer (PCa) is the second most frequent form of cancer (developed in men) after skin cancer [1]. PCa (like other cancers) is often painless in the initial stages. However, the cancerous cells in the prostate can grow progressively, leading even to death [2, 3]. To identify cancerous tissues, the most reliable and accurate examination is biopsy [4], where the pathologists and clinicians analyze the cell shapes and tissues to identify the underlying cancerous patterns and grade their severity. Clinically, Gleason scores are the extensively used procedure to grade the progression of the PCa [5]. Gleason scores for the cancerous pathologies range from 6 to 10, where 6 represents low-grade cancer, and 10 indicates the severe case. In 2014, the International Society of Urological Pathologists (ISUP) developed a simpler grading system for prostate cancer, dubbed the Grade Groups (GrG), which ranges from 1 to 5. The correlation between (GrG) and Gleason scores are presented in Table 1, where the GrG1 reflects the low-risk of prostate cancer (having Gleason score ≤ 6),

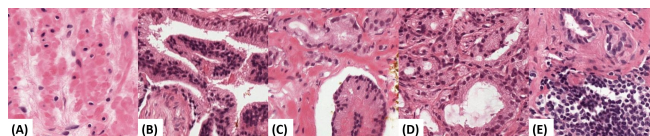


Fig. 1: Gleason patterns for PCa as per International Society of Urological Pathology (ISUP) grading system (A) GrG1, (B) GrG2, (C) GrG3, (D) GrG4, and GrG5.

and GrG5 reflects the high indication of prostate cancer in metastasis (with Gleason score ≥ 9).

Many researchers have worked on diagnosing cancerous pathologies from the histopathology and multi-parameter magnetic resonance imagery (mp-MRI) [6, 7]. The recent wave of these methods employed deep learning for segmenting the tumorous lesions [8] for the grading the cancerous tissues [9] (especially related to the prostate [10]). Towards this end, Wang et al. [11] conducted a study to showcase the capacity of deep learning systems for the identification of PCa (using mp-MRI) as compared to the conventional non-deep learning schemes. Smith et al. [12] identified clinically significant prostate cancer by screening prostate-specific antigens. As stated above, Gleason patterns are considered as a gold standard for identifying the cancerous pathologies [13] (especially the clinically significant PCa [5]). Moreover, Lucas et al. [14] presented a deep classification system to recognize Gleason patterns within prostate histopathological biopsies. Apart from this, Matoso et al. [5] presented an overview of the clinically significant PCa based upon the pathological findings. They concluded that for non-significant PCa, the criteria laid for the radical prostatectomy (RP) and needle biopsy are too strict (yet reliable at the same time). However, for clinically significant PCa, researchers (and clinicians) are focused on analyzing the percentage of Gleason pattern 4 over the rest. In addition to this, Wang et al. [15] proposed an autonomous local structure modeling framework that analyzes the glandular structures of the tissues within the histopathology images for the diagnosis and grading of PCa. Similarly, Arvaniti et al. [16] utilized MobileNet [17] driven Class Activation Maps (CAM) for the autonomous Gleason grading of the PCa tissues microarrays.

Although, many researchers have presented frameworks that

Table 1: ISUP Grading Scheme

Risk Level	Gleason Score	ISUP Grade
Low	Gleason Score ≤ 6	GrG1
Favorable	Gleason Score 7 (3+4)	GrG2
Unfavorable	Gleason Score 7 (4+3)	GrG3
High	Gleason Score 8	GrG4
High	Gleason Score 9 and 10	GrG5

can automatically grade the severity of PCa based upon the Gleason grading scores. However, to the best of our knowledge, there is no literature available which proposes a multi-scale autonomous framework to robustly extract the diverse ranging Gleason patterns within the Multi-Gigapixel whole slide images (WSI) to effectively grade PCa as per the clinical standards. To cater this, we present a single-staged segmentation framework capable of identifying the diverse ranging Gleason patterns (within the WSI) to give autonomous severity analysis of clinically significant PCa. To summarize, the main contributions of this paper are:

- This paper presents a novel encoder-decoder model containing a hierarchical decomposition block to analyze distinct feature representations generated from the WSI patches across various scales. These feature maps are then fused together to accurately extract the diversified Gleason patterns for grading the PCa as per the clinical standards.
- The proposed framework is penalized using the novel hybrid loss function L_h , which is driven through three-tiered objective functions to individually recognize the cluttered regions of the similarly styled Gleason tissues.

2. PROPOSED APPROACH

The block diagram of the proposed scheme is shown in Figure 2. To effectively recognize the Gleason tissues, first of all, we divide the candidate WSI scan into the set of non-overlapping patches. These patches are then passed to the proposed asymmetric encoder-decoder network that generates a pool of feature representations across various scales through its in-built hierarchical decomposition (HD) block. Afterward, the multi-scale feature representations are fused together, and this fused representation is passed to the decoder block that recognizes the cluttered Gleason patterns (within each patch) presenting the severity of PCa as per the clinical standards. Here, it should be also noted that instead of using a single loss function for training the encoder-decoder architecture, we used a hybrid loss function that penalizes the network for accurately recognizing the Gleason pattern through three-tiered objective functions. The detailed description of each block within the proposed framework is presented below:

2.1. Hierarchical Decomposition Block

Since many cellular regions within the WSI patches have similar contextual and textural properties [9]. Therefore, accurately differentiating them is a difficult task due to the high correlation between their feature representations and also due to the cluttered nature of different Gleason patterns. To address this, we present a novel HD block whereby we decompose the extracted feature representations from the encoder block across various scales and exploit distinct characteristics of each cellular region through atrous convolutions with variable dilation factors. Afterward, these distinct feature representations are pooled and fused together (via addition), as shown in Figure 2.

2.2. Hybrid Loss Function

In order to effectively train the proposed framework to recognize different similarly styled Gleason patterns (which gives the clinical grading of PCa), we have penalized the proposed framework using the hybrid loss function L_h , which is a linear combination of three-tiered objective functions as expressed below:

$$L_h = \frac{1}{N} \sum_{i=1}^N (\alpha_1 L_{c,i} + \alpha_2 L_{d,i} + \alpha_3 L_{ft,i}) \quad (1)$$

where

$$L_{c,i} = - \sum_{j=1}^C t_{i,j} \log(p_{i,j}) \quad (2)$$

$$L_{d,i} = 1 - \frac{2 \sum_{j=1}^C t_{i,j} p_{i,j}}{\sum_{j=1}^C t_{i,j}^2 + \sum_{j=1}^C p_{i,j}^2} \quad (3)$$

$$L_{ft,i} = \left(1 - \frac{\sum_{j=1}^C t_{i,j} p_{i,j}}{\sum_{j=1}^C (t_{i,j} p_{i,j} + \beta_1 t'_{i,j} p_{i,j} + \beta_2 t_{i,j} p'_{i,j})} \right)^{1/\gamma} \quad (4)$$

L_c denotes the categorical cross-entropy loss function, L_d denotes the dice loss function, and L_{ft} denotes the focal Tversky loss function [18] where γ indicates the focusing parameter. Moreover, $t_{i,j}$ denotes the true labels of the i^{th} example for the j^{th} class, $p_{i,j}$ denotes the predicted labels for the i^{th} example belonging to the j^{th} class, $t'_{i,j}$ denotes the true labels of the i^{th} example for the non- j^{th} class, $p'_{i,j}$ denotes the predicted labels for the i^{th} example belonging to the non- j^{th} class. Apart from this, N denotes the batch size, C denotes the total classes, $\alpha_{1,2,3}$ and $\beta_{1,2}$ are the loss weights. From Eq. 1, we can see that the L_h penalizes the proposed encoder-decoder network to correctly identify the Gleason cellular tissues (true positives) regardless of their cluttered nature, while simultaneously distinguishing between the false positives and false negatives. Furthermore, due to the γ factor, L_h give

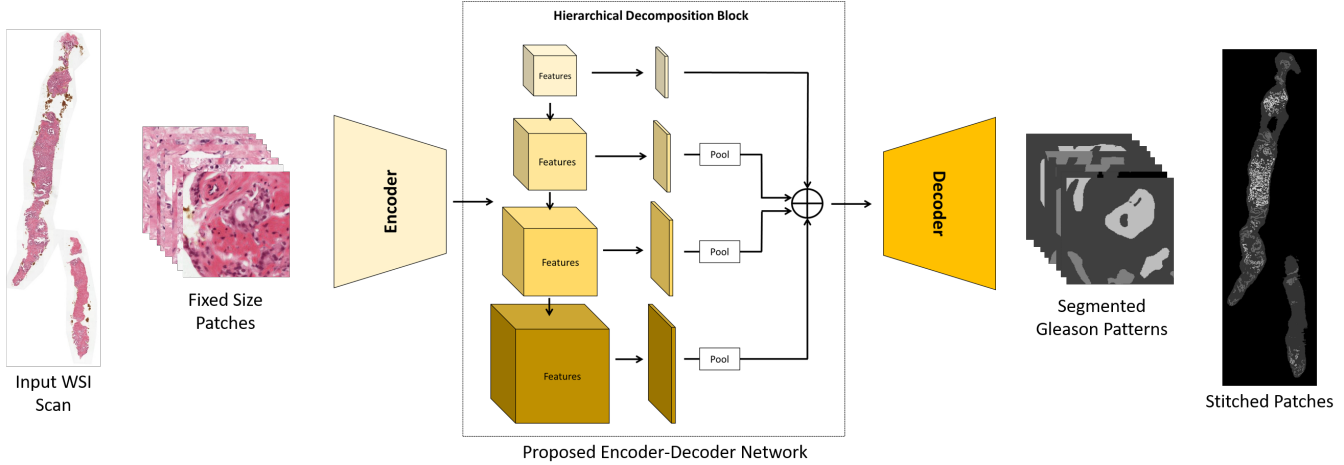


Fig. 2: Block diagram of the proposed framework. First of all, the candidate WSI is divided into fixed-size non-overlapping patches where each patch is passed to the proposed encoder-decoder model (trained via L_h). The proposed model then recognizes the cluttered instances of the Gleason cellular patterns which are stitched together to generate the segmented WSI representation for grading the severity of PCa.

Table 2: Performance evaluation of the proposed framework with different backbone networks. Bold indicates the best score while the second-best performance is underlined.

Backbone Network	mean IoU	mean DC
MobileNet [17]	0.3824	0.5532
VGG-16 [19]	0.3952	0.5665
ResNet-50 [20]	<u>0.4061</u>	<u>0.5776</u>
ResNet-101 [20]	0.4229	0.5944

more weigh to the hard-examples while discarding the contributions from the easy ones (which is very significant considering the highly imbalanced nature of positive and negative (background) pixel-level classes scattered patch-wise). Moreover, through rigorous experimentation, we found out the value of α_1 , α_2 , and α_3 to be 0.2, 0.2 and 0.6, respectively. Similarly, the value of β_1 , β_2 , and $1/\gamma$ are empirically chosen to be 0.7, 0.3, and 0.75, respectively.

3. EXPERIMENTAL SETUP

This section contains a detailed description of the dataset, training protocol, and the evaluation metrics which we have used in this study.

3.1. Dataset

The proposed framework was thoroughly evaluated on a total of 10,516 multi-gigapixel whole slide images of digitized H&E-stained biopsies acquired through the University of Louisville Hospital, USA. Each WSI scan was divided into the fixed patches of size $350 \times 350 \times 3$ (and there are around 71.7M patches in the complete dataset). Out of these 71.7M

patches, 80% were used for training and 20% were used for the testing purpose. Moreover, all the 10,516 WSI scans contain detailed annotations for the ISUP grades which have been marked by expert pathologists from the University of Louisville School of Medicine, USA.

3.2. Implementation Details

The proposed framework has been implemented using TensorFlow 2.3.1 and Keras APIs on the Anaconda platform with Python 3.7.8. The training was conducted for 25 epochs with a batch size of 1024 on a machine having Intel(R) Core(TM) i9-10940X@3.30GHz CPU, 160 GB RAM, and NVIDIA Quadro RTX 6000 GPU with CUDA v11.0.221, and cuDNN v7.5. Moreover, the optimizer used for the training was ADADELTA [21] with a learning rate of 1 and a decay rate of 0.95. The validation (after each epoch) was performed using 20% of the training dataset. The source code has been publicly released at: <https://github.com/taimurhassan/cancer>.

3.3. Evaluation Metrics

The proposed framework was evaluated using the Intersection-over-Union (IoU) and the Dice Coefficient (DC). IoU and DC both measures the ratio of the overlapped area (between the predicted results and the ground truth) w.r.t their union. The overlapped area is denoted as True positives (T_p), whereas the union is denoted as ($T_p + F_n + F_p$), yielding $\text{IoU} = \frac{T_p}{T_p + F_n + F_p}$. The difference between IoU and DC is that DC gives twice more weightage towards correctly classifying T_p , i.e., $\text{DC} = \frac{2T_p}{2T_p + F_n + F_p}$. Moreover, the mean IoU and the mean DC scores are computed by taking an average of IoU and DC scores for each class, respectively.

Table 3: Performance comparison of the proposed framework with popular scene parsing, encoder-decoder, and fully convolutional networks. All the models are driven through ResNet-101 [20] and L_h loss functions. Bold indicates the best performance while the second-best scores are underlined. The abbreviations are: M: Metric, J: IoU, D: DC, I: ISUP Grades, PF: Proposed framework, RN: RAGNet [22], PN: PSPNet [23], UN: UNet [24], and F8: FCN-8 [25].

M	I	PF	RN	PN	UN	F8
J	1	0.7240	<u>0.7031</u>	0.6819	0.6748	0.6532
	2	0.4180	0.3852	<u>0.3927</u>	0.3714	0.3581
	3	0.3708	0.3504	<u>0.3623</u>	0.3439	0.3246
	4	<u>0.3143</u>	0.3206	0.3091	0.2931	0.3028
	5	0.2876	<u>0.2793</u>	0.2638	0.2587	0.2479
	μ	0.4229	<u>0.4077</u>	0.4019	0.3883	0.3773
D	1	0.8399	<u>0.8256</u>	0.8108	0.8058	0.7902
	2	0.5895	0.5561	<u>0.5639</u>	0.5416	0.5273
	3	0.5409	0.5189	<u>0.5318</u>	0.5117	0.4901
	4	<u>0.4782</u>	0.4855	0.4722	0.4533	0.4648
	5	0.4467	<u>0.4366</u>	0.4174	0.4110	0.3973
	μ	0.5944	<u>0.5792</u>	0.5734	0.5594	0.5479

4. RESULTS

In this section, we present a detailed evaluation of the proposed framework through different experiments. For the first experiment, we coupled different pre-trained models (as an encoder) within the proposed architecture to showcase its generalizability and compatibility across various backbones. Here, we utilize popular backbone networks such as MobileNet [17], VGG-16 [19], ResNet-50 [20] and ResNet-101 [20] to derive the latent space representation of the candidate WSI patch. The choice of the backbone network does not affect much the overall performance of the proposed framework (as evident from Table 2). For instance, the best performing ResNet-101 [20] only leads the low-performing MobileNet [17] driven model by only 9.57% in terms of mean IoU and 6.93% in terms of mean DC. But since ResNet-101 [20] produced optimal results, we used it as the backbone model in the rest of the experiments.

In the second experiment, we compared the performance of proposed encoder-decoder network (driven through ResNet-101 [20]) with other popular models such as RAGNet [22], PSPNet [23], UNet [24], and FCN-8 [25], for extracting the Gleason patterns. Here, to make the comparison fair, all the segmentation models were trained using the same experimental protocols with the same backbone network, i.e., the ResNet-101 [20], and are trained via L_h loss function. From Table 3, we can see that the proposed framework achieves 3.59% performance gain over the second-best RAGNet [22] for extracting Gleason patterns. However, for extracting GrG4, the RAGNet is outperforming the proposed frame-

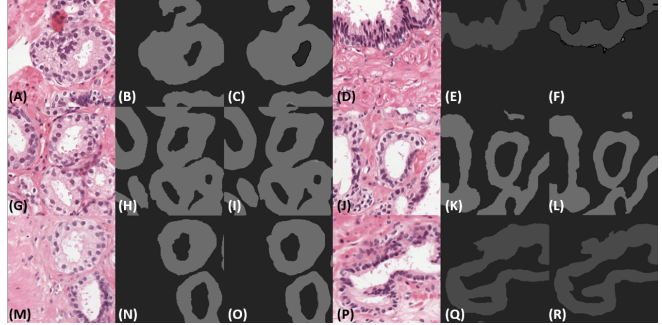


Fig. 3: Qualitative evaluation of the proposed framework. 1st and 4th column shown the original patches, 2nd and 5th column shows the ground truths, 3rd and 6th column shows the extracted results.

work by 1.96%. But considering the fact that the proposed framework achieves a significant margin from RAGNet [22] for extracting GrG1, GrG2, and GrG3, we believe the performance of the proposed framework is appreciable. Apart from this, for extracting GrG2 and GrG3, the PSPNet [23] is outperforming RAGNet [22] by 1.38% and 2.42%, respectively in terms of mean DC. From Table 3, we can also observe that the proposed framework produces the best results in differentiating low-risk and clinically significant PCa cases by achieving the best performance for extracting GrG1 and GrG5 groups as compared to popular segmentation models.

Lastly, we performed qualitative evaluations of the proposed framework as shown in Figure 3. Here, we can observe how effectively the proposed framework has extracted the Gleason patterns w.r.t the ground truths. For example, see the cases in (B)-(C), (H)-(I), and (N)-(O). Although, the proposed L_h ensured that the proposed framework robustly recognizes each Gleason pattern. But we still observed some false positives (e.g., see tiny regions in F), and some false negatives as well (e.g., see the smaller missed region in L). Although such incorrect predictions are rarely observed, they can be easily catered through morphological post-processing steps.

5. CONCLUSION

This paper presents an asymmetric encoder-decoder framework that leverages the hierarchical decomposition of latent feature representations across various scales to robustly recognize cluttered instance of Gleason cellular patterns which can objectively grade PCa as per the clinical standards. We have rigorously tested the proposed framework on a dataset consisting of 10,516 whole slide images, where we were able to outperform the state-of-the-art segmentation frameworks by 3.59%. In future, the proposed framework can be extended to perform Gleason patterns aware joint classification and grading of PCa. Furthermore, it can be used to extract other biomarkers for grading different cancerous pathologies.

Acknowledgement

This work is supported by a research fund from Khalifa University: Ref: CIRA-2019-047.

Compliance with Ethical Standards

This is a numerical simulation study for which no ethical approval was required.

6. REFERENCES

- [1] R. L. Siegel, K. D. Miller, and A. Jemal, "Cancer statistics, 2015," *CA: a cancer journal for clinicians*, vol. 65, no. 1, pp. 5–29, 2015.
- [2] A. Stangelberger, M. Waldert, and B. Djavan, "Prostate cancer in elderly men," *Rev Urol*, vol. 10, no. 2, pp. 111–119, 2008.
- [3] G. Litjens, O. Debats, J. Barentsz, N. Karssemeijer, and H. Huisman, "Computer-aided detection of prostate cancer in MRI," *IEEE Transactions on Medical Imaging*, vol. 33, no. 5, pp. 1083–1092, 2014.
- [4] M. N. Gurcan, L. E. Boucheron, A. Can, A. Madabhushi, N. M. Rajpoot, and B. Yener, "Histopathological Image Analysis: A Review," *IEEE Reviews in Biomedical Engineering*, October 2009.
- [5] A. Matoso and J. I. Epstein, "Defining clinically significant prostate cancer on the basis of pathological findings," *Histopathology*, 2019.
- [6] R. Cao, A. M. Bajgirani, S. A. Mirak, *et al.*, "Computer-aided detection of prostate cancer in MRI," *IEEE Transactions on Medical Imaging*, February 2019.
- [7] R. Kumar, R. Srivastava, and S. Srivastava, "Detection and Classification of Cancer from Microscopic Biopsy Images Using Clinically Significant and Biologically Interpretable Features," *Journal of Medical Engineering*, August 2015.
- [8] A. Nasim, T. Hassan, M. U. Akram, B. Hassan, and M. A. Shami, "Automated identification of colorectal gland sparsity from benign images," *International Conference on Image Processing, Computer Vision and Pattern Recognition*, 2017.
- [9] S. F. H. Naqvi, S. Ayubi, A. Nasim, and Z. Zafar, "Automated Gland Segmentation Leading to Cancer Detection for Colorectal Biopsy Images," *Future of Information and Communication Conference (FICC)*, 2019.
- [10] Z. Wang, C. Liu, D. Cheng, L. Wang, X. Yang, and K. T. T. Cheng, "Automated Detection of Clinically Significant Prostate Cancer in mp-MRI Images based on an End-to-End Deep Neural Network," *IEEE Transactions on Medical Imaging*, February 2018.
- [11] X. Wang, W. Yang, J. Weinreb, *et al.*, "Searching for prostate cancer by fully automated magnetic resonance imaging classification: deep learning versus non-deep learning," *Nature Scientific Reports*, 2017.
- [12] R. P. Smith, S. B. Malkowicz, R. Whittington, *et al.*, "Identification of clinically significant prostate cancer by prostate-specific antigen screening," *JAMA Internal Medicine*, 2004.
- [13] K. Nagpal, D. Foote, Y. Liu, P.-H. C. Chen, *et al.*, "Development and validation of a deep learning algorithm for improving gleason scoring of prostate cancer," *Nature Digital Medicine*, 2019.
- [14] M. Lucas, I. Jansen, C. D. Savci-Heijink, S. L. Meijer, O. J. de Boer, T. G. van Leeuwen, D. M. de Bruin, and H. A. Marquering, "Deep learning for automatic Gleason pattern classification for grade group determination of prostate biopsies," *Virchows Archiv*, 475, pp. 77–83, 2019.
- [15] D. Wang, D. J. Foran, J. Ren, H. Zhong, I. Y. Kim, and X. Qi, "Exploring automatic prostate histopathology image gleason grading via local structure modeling," *Conf Proc IEEE Eng Med Biol Soc*, 2016.
- [16] E. Arvaniti, K. S. Fricker, M. Moret, N. Rupp, T. Hermanns, C. Fankhauser, N. Wey, P. J. Wild, J. H. Rüschoff, and M. Claassen, "Automated Gleason grading of prostate cancer tissue microarrays via deep learning," *Nature Scientific Reports*, 2018.
- [17] A. G. Howard, M. Zhu, B. Chen, D. Kalenichenko, W. Wang, T. Weyand, M. Andreetto, and H. Adam, "MobileNets: Efficient Convolutional Neural Networks for Mobile Vision Applications," *arXiv:1704.04861*, 2017.
- [18] N. Abraham and N. M. Khan, "A Novel Focal Tversky loss function with improved Attention U-Net for lesion segmentation," *IEEE International Symposium on Biomedical Imaging (ISBI)*, 2019.
- [19] K. Simonyan and A. Zisserman, "Very Deep Convolutional Networks for Large-Scale Image Recognition," *arXiv preprint arXiv:1409.1556*, 2014.
- [20] K. He, X. Zhang, S. Ren, and J. Sun, "Deep Residual Learning for Image Recognition," *IEEE International Conference on Computer Vision and Pattern Recognition (CVPR)*, 2016.
- [21] M. D. Zeiler, "ADADELTA: An Adaptive Learning Rate Method," *arXiv:1212.5701*, 2012.
- [22] T. Hassan, M. U. Akram, N. Werghi, and N. Nazir, "RAG-FW: A hybrid convolutional framework for the automated extraction of retinal lesions and lesion-influenced grading of human retinal pathology," *IEEE Journal of Biomedical and Health Informatics*, 2020.
- [23] H. Zhao, J. Shi, X. Qi, X. Wang, and J. Jia, "Pyramid Scene Parsing Network," in *IEEE International Conference on Computer Vision and Pattern Recognition (CVPR)*, pp. 2881–2890, 2017.
- [24] O. Ronneberger, P. Fischer, and T. Brox, "U-Net: Convolutional Networks for Biomedical Image Segmentation." *International Conference on Medical Image Computing and Computer-Assisted Intervention (MICCAI)*, 2015.
- [25] J. Long, E. Shelhamer, and T. Darrell, "Fully Convolutional Networks for Semantic Segmentation," in *IEEE International Conference on Computer Vision and Pattern Recognition (CVPR)*, pp. 3431–3440, 2015.